Astron. Astrophys. 347, 127–136 (1999)

ASTRONOMY AND ASTROPHYSICS

Revised mass determination of the super massive Wolf-Rayet star WR 22⋆

J. Schweickhardt[1], **W. Schmutz**[2], **O. Stahl**[1], **Th. Szeifert**[1], **and B. Wolf**[1]

[1] Landessternwarte Heidelberg-Königstuhl, D-69117 Heidelberg, Germany
[2] Institut für Astronomie, ETH-Zentrum, CH-8092 Zürich, Switzerland

Received 8 February 1999 / Accepted 29 April 1999

Abstract. We analyze the orbital motion of the WN 7+abs + O binary WR 22 based on 88 high resolution optical spectra obtained in 1996. We determine a period of $P = 80.336 \pm 0.0013$ d and a radial velocity semi-amplitude $K_{\rm WR} = 70.6 \pm 0.8\,{\rm km\,s^{-1}}$ for the Wolf-Rayet star. By averaging six He I lines it is possible to detect the weak absorptions of the O companion. The spectral class of the O star is O 9 III (O 8–O 9.5) but the luminosity class is uncertain and brightness arguments indicate a luminosity class V. For the orbit of the O companion we derive $K_{\rm O} = 190 \pm 10\ {\rm km\,s^{-1}}$. This leads to a mass ratio $q = M_{\rm WR}/M_{\rm O} = 2.69 \pm 0.14$. We obtain masses of $55.3 \pm 7.3\ {\rm M}_\odot$ and $20.6 \pm 1.7\ {\rm M}_\odot$ for the WR and for the O star, respectively. Our mass determination revises down considerably the last published value for the mass of the Wolf-Rayet component but even with the new mass WR 22 remains "the most massive Wolf-Rayet star ever weighed".

Key words: stars: binaries: eclipsing – stars: binaries: spectroscopic – stars: early-type – stars: fundamental parameters – stars: individual: WR 22 – stars: Wolf-Rayet

1. Introduction

WR 22 (HR 4188, HD 92740, WN 7+abs) is one of the brightest Wolf-Rayet stars, $v = 6.40$, in the sky (Smith 1968; Schmutz & Vacca 1991). Lundström & Stenholm (1984) considered WR 22 to be a very probable member of the Carina OB1 association. With the distance modulus of Car OB1, $y_0 = 12.1$, WR 22 is also one of the intrinsically brightest Wolf-Rayet stars, $M_v = -6.85$ mag (Crowther et al. 1995).

The atmosphere of WR 22 contains a considerable amount of hydrogen, $X_{\rm H} \sim 40\%$ by mass (Hamann et al. 1991). The presence of hydrogen in the atmospheres of classical Wolf-Rayet stars is unusual but this property is common among WN 7+abs types (Crowther et al. 1995). The classification supplement "+abs" refers to absorption features of the upper Balmer series. These absorptions are intrinsic to the Wolf-Rayet star as they vary in phase with the emission lines. Although van der Hucht et al. (1981, 1988) list WR 22 as a single-lined spectroscopic binary (SB1) it is actually a double-lined binary. However, the absorptions from the companion are extremely weak and they can only be detected in spectra with a very high signal to noise ratio.

Several papers studied the orbit of this system in the last 25 years: Niemela (1973), Moffat & Seggewiss (1978), Conti et al. (1979), Niemela (1979), and Rauw et al. (1996). These analyses yield similar orbital parameters for the WR component but the challenge of this system is to find the velocity curve of the faint companion. Conti et al. (1979) detected some extra absorption dips in the Balmer and He II lines. Their tentative conclusion was: $q = M_{\rm WR}/M_{\rm O} \sim 2$. Niemela (1979) derived masses of $M_{\rm WR} \sin^3 i = 64\ {\rm M}_\odot$ and $M_{\rm O} \sin^3 i = 24\ {\rm M}_\odot$. The latest determination with improved observational data was carried out by Rauw et al. (1996). Their result was $M_{\rm WR} \sin^3 i = 71.7\,{\rm M}_\odot$ and $M_{\rm O} \sin^3 i = 25.7\ {\rm M}_\odot$.

All analyses agree in that WR 22 is the most massive Wolf-Rayet star ever weighed and as such, this star warrants special attention.

The light curve of WR 22 shows eclipses when the WR star is in front (Balona et al. 1989, Gosset et al. 1991). Because WR 22 is a rather wide binary, $P \approx 80$ days, the eclipse implies an inclination angle close to $90°$. The eclipse depth of 0.07 to 0.09 mag allows to conclude that the companion must also be a luminous object with a brightness difference relative to the Wolf-Rayet star of less than $\Delta M_V < 2.8$ mag (Rauw et al. 1996).

In the present paper we study the orbital motion of WR 22 based on a large data set of new spectroscopic observations. The observations are described in the next section and in Sect. 3 we derive the period by combining our data with that of Moffat & Seggewiss (1978) and Conti et al. (1979). In Sects. 4 and 5 we derive the velocity amplitudes of both components and in Sect. 6 the remaining orbital elements. The spectral classification of the companion is discussed in Sect. 7. In the last section we compare our results with previous determinations.

2. Observations and data reduction

We obtained our data in a 104-day observing campaign from January 19 to May 1, 1996 (JD 2 450 101 to JD 2 450 204).

Send offprint requests to: (jschweickhardt@lsw.uni-heidelberg.de)

⋆ Based on observations collected at the European Southern Observatory at La Silla, Chile. ESO proposals Nr. 56.D-327 and 57.D-517.

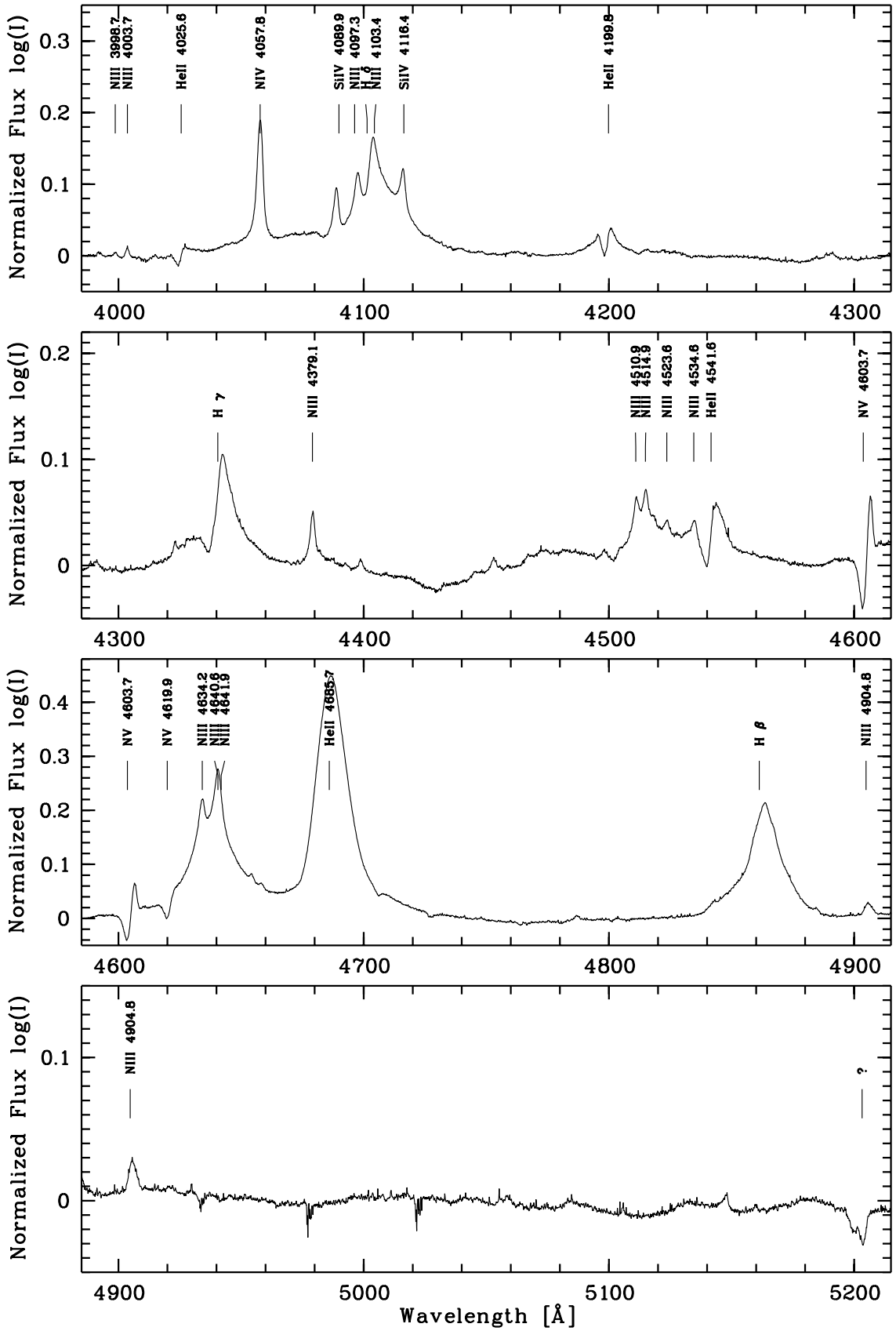

Fig. 1. Average spectrum of WR 22 in the blue wavelength region. Before averaging all spectra were corrected for the orbital motion of the WR star. Pay attention to the different intensity scales.

WR 22 was observed once a night with only few gaps. We have collected a total of 84 spectra in the blue wavelength region and 88 in the red, recorded simultaneously with the fiber fed Echelle spectrograph HEROS (Heidelberg Extended Range Optical Spectrograph, Kaufer 1998) at the ESO 50 cm telescope. The light is divided into a blue and red path after the Echelle grating, then cross-dispersed with a grating for each channel, and finally, the spectrum is recorded on two CCDs. The total wavelength coverage of the instrument is from 3500 Å to 8600 Å. The two pixel resolution is $R = 20\,000$. During an observing night typically every 2 hours lamp spectra are recorded for flat fielding and wavelength calibration. The exposure time was about 2 hours. For the data reduction we used a specially adapted version of the ESO-MIDAS Echelle context (Stahl et al. 1995).

In Fig. 1 we show the average spectrum of part of the blue wavelength region. Before averaging we corrected all spectra for the orbital motion of the WR star.

To verify the stability of the wavelength calibration we have measured the radial velocities of interstellar Ca II $\lambda 3934$ and Na I $\lambda 5890$ in the spectra of WR 22. We find that the scatter in both channels agrees with the nominal accuracy of the instrument ($\sigma_{\rm CaK} = 0.44\,{\rm km\,s^{-1}}$, $\sigma_{\rm NaD_2} = 0.19\,{\rm km\,s^{-1}}$) derived by Kaufer et al. (1997). This is more than a factor of 10 less than the standard deviation of the velocity measurements from the orbital fit and therefore, there is no significant instrumental contribution to the error of the results.

The signal to noise ratio of each recorded spectrum is $S/N \approx 50$ at 4000 Å and $S/N \approx 100$ at 6400 Å. The Echelle ripples are removed with the flat-field lamp response. Remaining ripple signatures are of the order of 1%. The spectra are normalized by a spline fit through selected wavelength points, roughly separated by 250 Å. These points are chosen to be free of emission lines as good as possible but in the blue wavelength region, the crowding of the lines is severe that there, we possibly do not reach the true continuum level.

3. The orbital period

Niemela (1973) collected 14 spectra over a two-year period and she determined an orbital period of 1.04 days. Moffat & Seggewiss (1978) used 25 spectra obtained in the years 1970, 1976, and 1977 and they found a best solution of 80.35 days. Conti et al. (1979) also derive 80.35 days. The latter combined the old data from Niemela (1973) with 83 additional spectra collected from 1972 to 1977. Finally, a period of 80.325 days was computed by Rauw et al. (1996). They collected more than 200 spectra over eight years and also included photometric data.

We combine the radial velocities from Moffat & Seggewiss (1978, Table 1) and Conti et al. (1979, Table 3) with our values, covering a time span of 26 years. For a better comparison, we only select data of apparently unblended lines which implies that we restrict our analysis to the lines N IV $\lambda 4057.8$ and He II $\lambda 4685.7$ listed by both authors, and N V $\lambda 4603.7$ measured only by Moffat & Seggewiss (1978).

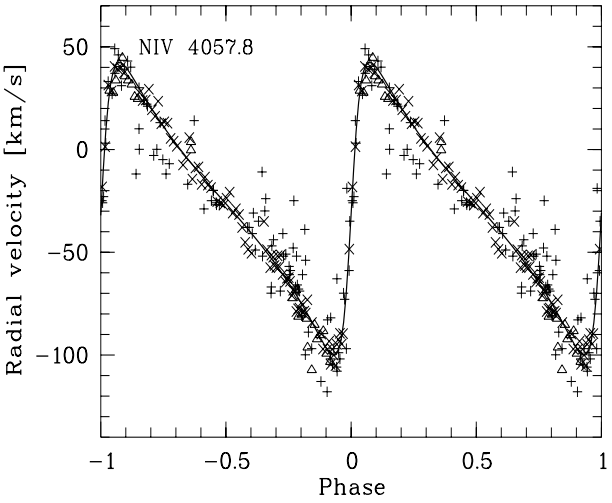

Fig. 2. Observed radial velocities of the N IV 4057.8 emission line. Crosses denote measurements of HEROS during 1996. The plus signs represent data obtained between 1972 and 1977 by Conti et al. (1979) and the triangles indicate values obtained 1970, 1976, and 1977 collected by Moffat & Seggewiss 1978. The line is the orbital solution fitted to the combined data set with a period $P = 80.336$ days.

In order to join the different data sets we first correct for differences in the resulting systemic velocities and then we derive the period from the combined set of radial velocities. Because the other orbital parameters are more accurately derived from the radial velocities of our data set we adopt e, ω, T_0, γ and K from the analysis presented below. Fig. 2 shows the best fit for N IV $\lambda 4057.8$ to the combined data set. Crosses ($\times$) denote the HEROS measurements, triangles mark the data taken from Moffat & Seggewiss (1978) (shifted by $\Delta\gamma = -4.3\ {\rm km\,s^{-1}}$), and plus signs indicates the values from Conti et al. (1979) (shifted by $\Delta\gamma = -1.9\ {\rm km\,s^{-1}}$).

We find periods of $P = 80.3354$ days for N IV $\lambda 4057.8$, $P = 80.3350$ days for He II $\lambda 4685.7$, and $P = 80.3375$ days for N V $\lambda 4603.7$. As the quality of all fits are similar, we adopt the mean for our orbital period determination: $\bar{P} = 80.336 \pm 0.0013$ days.

4. The velocity amplitude of the WR star

Niemela (1979) and Conti et al. (1979) analyzed several emission and absorption lines and finally decided to use the narrow emission lines of nitrogen and silicon to compute the WN 7 orbit: Conti et al. (1979) derived $K_{\rm WR} = 77 \pm 2\,{\rm km\,s^{-1}}$ and Niemela (1979) concluded $K_{\rm WR} = 74 \pm 2\,{\rm km\,s^{-1}}$. Moffat & Seggewiss (1978) studied several lines but they decided to base their determination of the WR orbit also on N IV $\lambda 4057.6$. They obtained $K_{\rm WR} = 70\,{\rm km\,s^{-1}}$. The N IV line was also the choice of Rauw et al. (1996) and they determined $K_{\rm WR} = 72.3 \pm 1.0\,{\rm km\,s^{-1}}$.

We analyzed more than 15 strong emission and absorption features. The full width at zero intensity of the emission lines range from ± 300 to $\pm 1\,700 {\rm km\,s^{-1}}$, depending on the ionization stage, multiplet structure or blending effects. In order to measure

Table 1. Orbital elements determined from the radial velocity variations of several nitrogen lines (in emission if not otherwise indicated). A period of $P = 80.336$ d is assumed.

Parameter	N III $\lambda4097$	N III $\lambda4379$	N III $\lambda4634$	N III $\lambda4640$	N IV $\lambda4058$	N IV $\lambda6220$	em N V[a] $\lambda4604$	abs N V[b] $\lambda4604$
intensity	0.19	0.10	0.37	0.58	0.47	0.11	0.18	-0.13
FWHM [Å]	3.75	2.84	4.20	6.26	2.85	2.38	2.39	4.38
γ[c] [km s^{-1}]	-19.0	-11.2	-44.9	-26.7	-27.5	-13.4	145.7	0.6
e	0.588	0.587	0.604	0.613	0.600	0.596	0.587	0.591
ω [deg]	267.3	269.9	268.3	269.8	268.0	265.8	268.1	263.4
T_0 JD 2 400 000.5+	50 127.04	50 127.25	50 126.85	50 127.05	50 126.90	50 126.70	50 126.82	50 126.51
K [km s^{-1}]	70.05	71.92	69.72	70.51	71.10	70.43	71.32	66.76
σ_{O-C} [km s^{-1}]	12.4	8.0	6.9	6.5	4.4	5.3	6.0	10.1

[a] P Cyg profile: simultaneous double-Gauss fit to absorption and emission. Orbit analysis of the emission component.
[b] as [a] but orbit analysis of the absorption component.
[c] Reference wavelengths are: 4097.3, 4379.1, 4634.2, 4640.6, 4057.8, 6219.9, and 4603.7

the radial velocity of a line we have fitted Gaussian profiles to the emission and absorption lines. For the narrowest nitrogen emission lines, a combination of a Gaussian and Lorenz profile was tried to improve the fit to the profile wings. As we did not find a significant difference on the resulting orbit (except for a small shift for the system velocity γ), we use Gaussian profiles.

For the determination of the orbit we minimize the sum of the squared deviations by varying simultaneously all free parameters (γ, e, ω, T_0 and K) except the period which we set to the value derived in Sect. 3: $P = 80.336$ days. In addition to the orbital elements the fit procedure yields also the rms deviation. For every line, we tried several line fits with both fixed and variable line width and intensity but we obtain the smallest σ_{O-C} for the orbital solutions fitted with the profiles set to their average shape.

In Table 1 we give line widths (FWHM), intensities in continuum units, and orbital solutions obtained for individual lines of nitrogen. The velocity amplitudes of the nitrogen lines show a uniform behavior. From the medium ionized N III to the highly ionized N V lines, we find $K_{WR} = 70.2\,\mathrm{km\,s^{-1}}$ with a standard deviation of 1.6 $\mathrm{km\,s^{-1}}$. Only the orbital solution of the P Cygni absorption of N V $\lambda4604$ deviates from the results of the other nitrogen lines. but the fit to this line is also characterized by significantly larger residuals. As an illustration of the good quality of these orbital solutions, we show in Fig. 3 the fit to the N IV $\lambda6219.9$ emission line.

The upper Balmer lines are in absorption, starting with H ϵ. The best Gaussian fits were possible for H 10 and H 9. Both lines show a significantly higher scatter than the nitrogen solutions. The velocity amplitudes of these Balmer lines are lower than the values of the nitrogen solutions. This effect was also mentioned by Moffat & Seggewiss (1978) and Conti et al. (1979). A possible explanation for this behavior was already given by the previous authors: The companion of the Wolf-Rayet star (an O star, see Sect. 7) has Balmer absorption lines moving in antiphase to the WR absorptions. So, the absorptions of the WR star are disturbed and a smaller velocity amplitude results.

In Fig. 4 we plot the measured velocities of the H 9 absorption together with the fitted orbit (dashed line) and the orbital solution as derived from the nitrogen lines (solid line, with adjusted γ value).

Interestingly, the two solutions deviate significantly only for positive velocity displacements. These are the phases when the P Cygni absorption of the WR star, blue-shifted by its nature, is red-shifted by the orbital motion to coincide with the O star absorption.

The parameters of the lower Balmer emission lines show a behavior more similar to the nitrogen lines. The scatter of the orbital analysis is improving especially for H α. But the main difficulty for these lines was the line fitting procedure. The line profiles of these lines are far from being simple Gaussian profiles. Furthermore, because of the neighborhood of the H δ line to Si IV $\lambda4088.9$ (P Cyg profile), N III $\lambda4097.3$, and Si IV $\lambda4116.1$, we fitted the whole region simultaneously with five Gaussians, four emissions and one absorption. Therefore, we are afraid that the fit procedure did not find the line centers with high precision. This problem affects the resulting K value and therefore, we decide not to include these emission lines in the K determination.

In Table 2 we also list orbital parameters derived for three He II lines. We fitted those lines showing a P Cygni profile with a double-Gauss fit consisting of an absorption and an emission component. In Table 2 we only list the result of the absorption component because their rms scatter is much smaller than those of the emissions.

For He II $\lambda4685.7$ a simple Gaussian fit was used. The orbital determination leads to a very small error, but for this line we had similar problems as for the Balmer emission lines: the profile does not look very Gaussian, so it is probable that the line fit determines not exactly the line center.

Finally, the orbital analysis with the Si IV $\lambda4088.9$ emission line is given. As mentioned above, we used a simultaneous fit of four emission and one absorption component for the 4100 Å region. The emission component of this P Cyg profile shows a smooth behavior and yields a good fit, but the absorption feature

Table 2. Orbital elements determined from the radial velocity variations of several H, He, and Si lines (in emission if not otherwise indicated). A period of $P = 80.336$ d is assumed.

Parameter	abs H10 λ3798	abs H9 λ3835	Hδ λ4102	Hβ λ4861	Hα λ6563	abs He II[a] λ4200	abs He II[a] λ4541	He II λ4686	Si IV λ4089
γ[b] [km s^{-1}]	7.5	-122.2	155.7	120.2	38.7	-142.3	-140.8	56.9	-24.6
e	0.652	0.498	0.539	0.612	0.614	0.586	0.576	0.600	0.640
ω [deg]	227.7	226.4	252.4	263.3	268.2	267.4	258.3	268.6	272.9
T_0 JD 2 400 000.5+	50 122.89	50 122.55	50 125.77	50 126.33	50 126.85	50 126.91	50 125.80	50 126.87	50 127.30
K [km s^{-1}]	63.43	52.39	75.71	81.89	74.60	67.66	78.41	73.80	76.90
σ_{O-C} [km s^{-1}]	23.1	22.8	18.1	13.9	6.5	12.1	8.8	4.1	9.2

[a] P Cyg profile: simultaneous double-Gauss fit to absorption and emission. Orbit analysis of the absorption component.
[b] Reference wavelengths are: 3797.9, 3835.4, 4101.7, 4861.3, 6562.8, 4199.8., 4541.6, 4685.7, and 4088.9

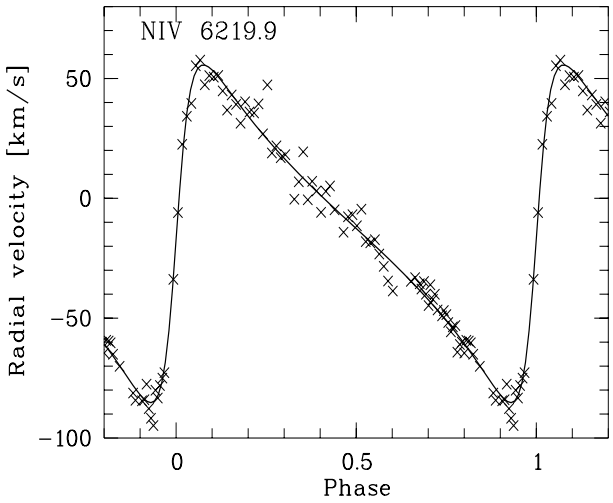

Fig. 3. Phase diagram of the radial velocities of the N IV λ6219.9 emission line. Crosses denote our observations and the solid line indicates the orbital solution with the parameters given in Table 1

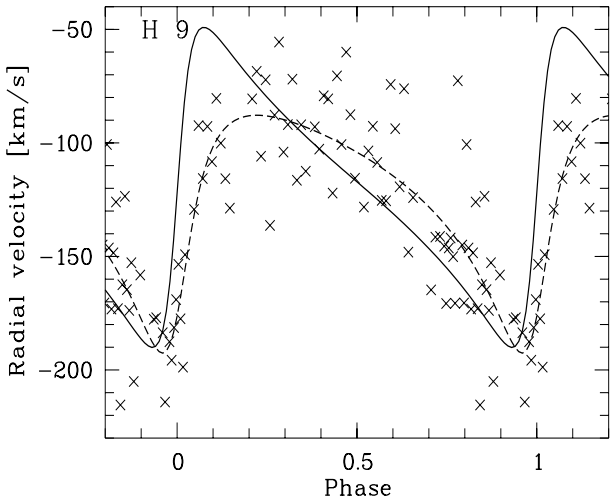

Fig. 4. Phase diagram of the radial velocities of the H 9 absorption line. Crosses denote our observations and the dashed line indicates the orbital solution with the parameters given in Table 2. The orbital solution of the nitrogen lines (see Table 1), with adjusted γ, is shown by the solid line. The H 9 line is obviously distorted most at positive velocity displacements, when the P Cygni absorption of the WR star interferes with the O star absorption.

is variable with time with large deviations from the orbital solution. The fit to the emission component yields a small scatter but with a significantly higher velocity amplitude K than for the nitrogen lines. We suspect that the emission is disturbed by the systematically variable absorption profile altering the orbital solution.

Because of the much better quality of the nitrogen line fits, we base the WR orbital elements on these lines only. An averaging of the semi-amplitudes of all nitrogen emission features listed in Table 1, except em N V λ4603.7, yields $\bar{K}_{\rm WR} = 70.6 \pm 0.8$ km s^{-1}. For the internal precision of our amplitude determination we have adopted the standard deviation of the 6 lines. However, we suspect that the deviations are not random but systematic and therefore, we do not reduce the error of the mean amplitude by the square root of the number of measurements.

5. The velocity amplitude of the companion

A careful inspection of the spectra reveals that there are extra absorption dips that move in anti-phase at the wavelengths of Balmer lines and He II lines (Conti et al. 1979; Niemela 1979; Rauw et al. 1996).

Absorptions from He I lines are the strongest feature of the companion. But even for those we needed a higher S/N than that of a single spectrum of our observations in order to be able to measure the radial velocities.

We therefore use the large number of observed spectra to our advantage. We constructed so-called dynamical spectra. First, we rebin the spectra to a velocity scale with the zero-point set to the laboratory wavelength of the He I line. On these dynamical spectra, the movement of some He I absorptions is easily detectable. To get a clearer view, in a second step we average six of the He I dynamical spectra to improve the signal-to-noise. In Fig. 5 the average of the dynamical spectra of the six lines He I $\lambda\lambda$3819.7; 4143.8; 4387.9; 4471.5; 4713.3; 4921.9 is shown. Here the intensities are coded in grey scales (from black = absorption to white = emission). Above the dynamical

Table 3. Orbital elements determined from the data shown in Fig. 5. Columns 1A and 1B are calculated with radial velocities obtained by a Gaussian fit to every spectrum. In Columns 2A and 2B we used velocities measured by eye inspection. Finally, Columns 3A and 3B show the orbital determination obtained by a two-dimensional fit to the data. Fixed parameters are marked with @.

Parameter	1A	1B	2A	2B	3A	3B
γ	1.6	-5.1	14.9	33.1	-2.7	-3.0
e	0.46	0.60@	0.56	0.60@	0.59	0.60@
ω [deg]	83.9	88.2@	89.1	88.2@	89.1	88.2@
T_0 JD 2 400 000.5+	50 128.3	50 127.0@	50 128.9	50 127.0@	50 127.4	50 127.0@
K [km s^{-1}]	166.8	192.3	189.6	162.6	189.6	189.9
$\sigma_{\mathrm{O-C}}$ [km s^{-1}]	21.7	27.1	21.1	49.8	19.6	20.6

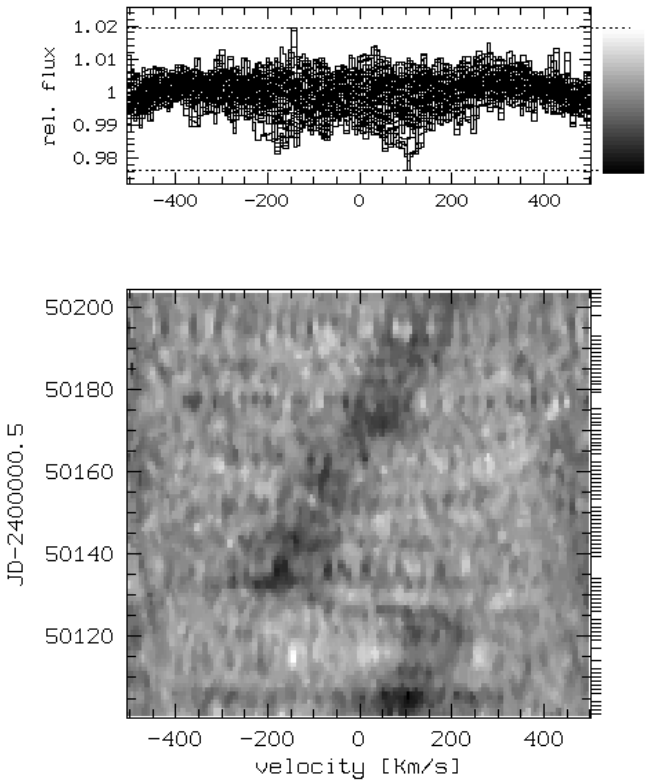

Fig. 5. Dynamical spectrum of a mean He I absorption line of the O companion. The spectra of He I $\lambda\lambda$3819.7; 4143.8; 4387.9; 4471.5; 4713.3; 4921.9 are averaged in velocity units.

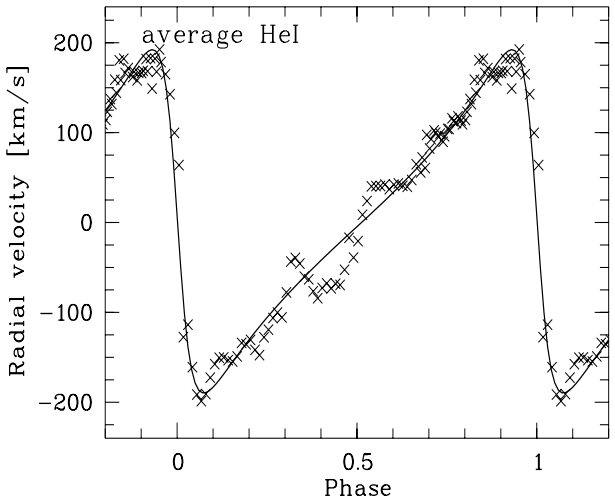

Fig. 6. Phase diagram of the radial velocities of the average He I absorption line of Fig. 5. Crosses denote the radial velocities measured with an iterative method (see text). The solid line indicates the orbital solution with the parameters given in Table 3, Column 3C.

spectra, all spectra are plotted within the velocity range and an appropriate intensity interval. The cut values used for the grey-scale representation are indicated by the two dashed lines and the grey scale itself is shown at the right-hand side (for further information see Kaufer et al. 1996). To improve the contrast, we applied a median filter to the image in x- and y- direction with a radius of three pixels. In the resulting frame, the eccentric movement of the absorption line is clearly visible.

We used three methods to determine the orbital parameter of the companion. First, we fit a Gaussian absorption profile with free parameters independently to every single spectrum. The result is not satisfactory because in many cases the fitting procedure did not locate the absorption correctly. Orbital parameters derived with this method are given in Table 3. There are two columns, Column 1A for which only the Period P is fixed and Column 1B, where we fixed P, e, ω_{O}, and T_0 (see Sect. 6). The fixed values are indicated by the @ symbol.

Our second method is an inspection by eye. The disadvantage of this method is clear: it is subjective, but the eye has a good ability to follow the movement of the absorption line over the complete orbit. The orbital solutions for this method are given in Columns 2A (fixed P) and 2B (fixed P, e, ω and T_0).

Third, we used a method which models the entire dynamical spectrum, but is based on a given constant Gaussian profile at all orbital phases. The free parameters are the profile parameters of the Gaussian fit to the average profile and the radial velocities v_r of the subsequent phase bins. The non-linear χ^2 optimization problem is solved with the Levenberg-Marquardt routines of the numerical recipes (Press et al. 1992). About 10 iterations are needed to reach convergence. In Table 3 (Columns 3A and 3B), the orbital solutions are given. Fig. 6 shows the orbital solution of Column 3B. Crosses denote the measured radial velocities obtained with our iterative method. The one-sigma errors of the velocities are of the order of 20 km s^{-1}.

A comparison of the results from the different methods shows that we get similar results. In addition, we find that the

orbital solutions 1A, 2A, 3A yield parameters that agree with the $e, T_0, \omega_{\rm O} = \omega_{\rm WR} - 180^{\rm o}$ of the WR star orbit (see Table 1). This strengthens our confidence in the measured radial velocities of the O companion. However, the errors of the parameters from the O star orbit are significantly larger than those from the WR star. Therefore, we favor the orbital solutions with corresponding parameters defined by the Wolf-Rayet orbit. We regard the result of method 3B to be the most reliable one: $K_{\rm O} = 190 \pm 10$ $\mathrm{km\,s^{-1}}$. It is difficult to assess an error for this amplitude. The quoted value is chosen rather arbitrarily as half of the rms scatter of the data.

6. The eccentricity, periastron angle and date, and systemic velocity

The former studies of the orbit of WR 22 did not yield consistent results for the eccentricity. Niemela (1979) derived $e = 0.61 \pm 0.02$ for some emission lines and $e = 0.64 \pm 0.02$ for absorption features. Moffat & Seggewiss (1978) got a best solution of $e = 0.55 \pm 0.05$ and Conti et al. (1979) $e = 0.64 \pm 0.01$ for emission and $e = 0.62 \pm 0.02$ for absorption lines. Extreme values for certain lines are also given by Conti et al. (1979): $e = 0.45 \pm 0.05$ for the N V $\lambda\lambda 4603; 4619$ absorption lines and $e = 0.72 \pm 0.02$ for the He II $\lambda 4686$ emission line. Finally, Rauw et al. (1996) measured $e = 0.559 \pm 0.009$ from the N IV $\lambda 4058$ emission line.

Fortunately, our good coverage of the orbital phase defines the radial velocity curve more accurately and we obtain a consistent value for the eccentricity from different lines. Only the Balmer lines H 10, H 9 and H δ (see Table 2) deviate significantly (e.g. H 10: $e = 0.65$; H 9: $e = 0.52$). As pointed out above, we are of the opinion that this is a signature of the disturbance by the absorption lines of the O companion. Because of the better quality of the nitrogen emission line analyses (see Table 1), we adopt the mean eccentricity of these solutions, excluding again the emission component of N V $\lambda 4603.7$: $\bar{e} = 0.598 \pm 0.010$. From the same emission lines of Table 1 we calculate a mean periastron angle of $\bar{\omega}_{\rm WR} = 268.2 \pm 1.6\,^\circ$. The mean periastron date of these nitrogen lines is $\bar{T}_0 = \mathrm{JD}\ 2\,450\,127.47 \pm 0.14$ (Table 1). The ephemeris for the time of periastron passage is thus

$$\mathrm{JD(periastron)} = 2\,450\,127.47 + 80.336E\,. \qquad (1)$$

In this paper all phases are calculated with Eq. 1.

WR 22 is an eclipsing system (Balona et al. 1989, Gosset et al. 1991) and therefore it is of interest to calculate the conjunction time from the orbital solution. Because the periastron angle is very close to 270° the WR star is in front of its companion only 0.08 days after periastron passage, i.e. at orbital phase $\phi = 0.0010$. Thus, the ephemeris for the eclipse of the O star by the WR star is

$$\mathrm{JD(WR\ in\ front)} = 2\,450\,127.55 + 80.336E\,. \qquad (2)$$

The other conjunction with the O star in front is at orbital phase $\phi = 0.516$.

There are two published dates for observed eclipses: JD 2 447 235.8 and the JD 2 447 958.6 (Gosset et al. 1991). Using Eq. 2 we predict mid eclipse for JD 2 447 235.5 and JD 2 447 958.5 with $E = -36$ and -27, respectively. The differences to the published eclipse dates are not significant because for both dates the time of mid eclipse cannot be determined accurately.

The transverse velocities during eclipse are 112.8 $\mathrm{km\,s^{-1}}$ and 300 $\mathrm{km\,s^{-1}}$ for the WR and O star, respectively, and with the radius of the WR star, $R_{2/3} = 28.5$ $\mathrm{R_\odot}$ (Crowther et al. 1995), and a radius of a O 9 III star, $R_* = 12$ $\mathrm{R_\odot}$ (Howarth & Prinja 1989), we predict an eclipse duration of 15.3 h from 2nd to 3rd contact and 38 h from 1st to 4th contact.

The center of WR emission lines is usually shifted by an amount that depends on the line. In general, without an atmosphere code, it is not even possible to predict whether the line center is red-shifted or blue-shifted. Consequently, it is not possible to use WR lines to determine the systemic velocity. Therefore, only O star absorption should be used but unfortunately, we could not detect individual O star lines in the individual, un-averaged spectra. Using the co-added He I lines we find the γ values listed in Table 3. Excluding method 2, we derive $\gamma = -3\,\mathrm{km\,s^{-1}}$. Measuring the line centers of individual He I lines in the average spectrum (corrected for the orbital motion of the O star, see Fig. 7), we get velocities from $-20\,\mathrm{km\,s^{-1}}$ to $+37\,\mathrm{km\,s^{-1}}$.

An interesting constraint is introduced by N V$\lambda 4604$. Because this line has a P Cygni profile the absorption is certainly not red-shifted. Using the orbital parameters of the WR star derived above, we find for the absorption component $\gamma_{\rm N\,V} = +1.1\,\mathrm{km\,s^{-1}}$. We conclude that the systemic velocity of WR 22 is zero with an uncertainty of about 15 $\mathrm{km\,s^{-1}}$.

7. Spectral classification of the companion

To get the spectral type and the luminosity class of the companion, it is necessary to measure the equivalent widths of its lines. This is not straightforward because the absorption lines are weak and hard to detect in our spectra. Furthermore, the absorption lines of the companion are strongly blended with WR lines.

In Figs. 7 and 8 we show the mean of all spectra after correcting for the orbital motion of the O companion for the lines He I $\lambda 4471$ and He II $\lambda 4541$.

Because the He II $\lambda 4541$ absorption is not well defined even in the averaged spectrum we assumed for the He II line the same width of 124 $\mathrm{km\,s^{-1}}$ as we measure for He I $\lambda 4471$. We derive $W_\lambda(4471) \sim 0.035$ Å and $W_\lambda(4541) \sim 0.016$ Å. It's difficult to determine the errors of these values. We estimate for both lines an uncertainty of ± 0.005 Å, yielding relative errors of 15% and 30% for the He I and He II line, respectively. Using the quantitative classification system of Conti & Alschuler (1971) and Mathys (1988), $\log_{10} W'_\lambda = \log_{10}(W_\lambda(4471)/W_\lambda(4541)) \sim 0.35 \pm 0.2$, we obtain O 9 for the spectral type of the O star with an uncertainty range O 8–O 9.5. This does not agree very well with Rauw et al. (1996) who derived O 6.5–O 8.5. The reason

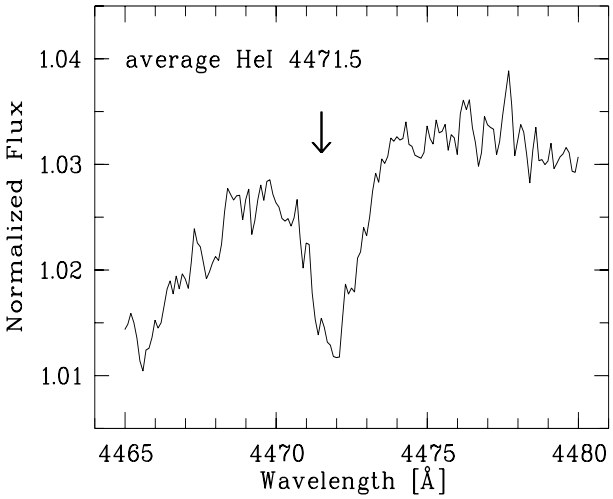

Fig. 7. Average spectrum of WR 22 in the 4471 Å region. Before averaging all spectra were corrected for the orbital motion of the O star. The He I $\lambda 4471.5$ absorption (marked with ↓) is clearly visible.

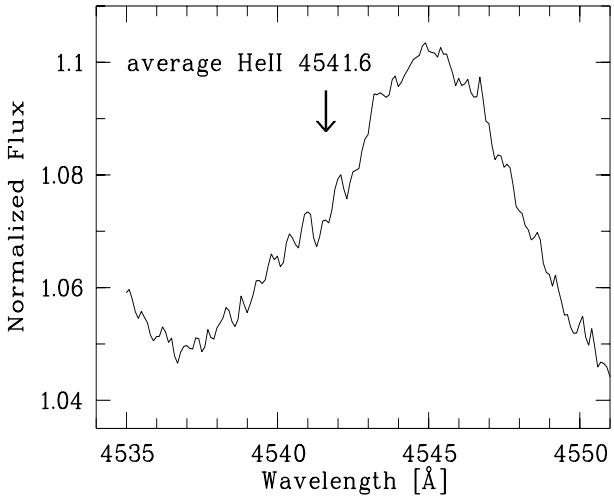

Fig. 8. Average spectrum of WR 22 in the 4541 Å region. Before averaging all spectra were corrected for the orbital motion of the O star. The He II $\lambda 4541.6$ absorption is visible on the blue shifted wing of the WR emission (marked with ↓).

for our later type is that in our specra the $W_\lambda(4541)$ absorption is weaker.

In order to derive the luminosity class we investigate the lines Si IV $\lambda 4089$ and He I $\lambda 4143$. Again, we assume a width of 124 $\mathrm{km\,s^{-1}}$ before fitting the features with a Gaussian profile. We find $W_\lambda(4089) \sim 0.025$ Å and $W_\lambda(4143) \sim 0.015$ Å. Using the criteria of Conti & Alschuler (1971) we derive $\log_{10} W''_\lambda = \log_{10}(W_\lambda(4089)/W_\lambda(4143)) \sim 0.22$, which leads to a luminosity class III.

The absolute visual brightness of the WR 22 system is given by Crowther et al. (1995) as $M_v = -6.85$ mag. With the depth of the eclipse it is possible to estimate a lower limit to the brightness of the companion. Gosset et al. (1991) observe a variation of magnitude in the Strömgren system of $\Delta b = 0.071$ and $\Delta(b-y) = -0.012$. This leads to $\Delta y = 0.083$. Assuming a total eclipse of the O star, the Wolf-Rayet star has a brightness of $M_v^{\mathrm{WR}} = -6.77$ mag and the O star $M_v^{\mathrm{O}} = -4.02$ mag.

A typical O 9 III star has an absolute magnitude of $M_V^{\mathrm{O}} = -5.1$ (Howarth & Prinja 1989). Therefore, the eclipse could be either only partial, i.e. only 37%, or our derivation of the luminosity class is not correct. The brightness of an O 9 V star is $M_V = -4.2$ which fits nicely to the lower limit derived above for the visual magnitude of the O companion.

A luminosity classification should follow from spectral features only and it is not really correct to use the absolute brightness, especially as distance and reddening are also not very well known. However, our detection of the classification lines are marginal and we do not trust the spectroscopic luminosity class. Clearly, spectra with a higher signal to noise are required for a better assessment of the luminosity class of the O star.

8. Discussion

In Table 4 we summarize the physical parameter of WR 22 and in Table 5 we compare our orbital elements with previous determinations. We confirm that the mass ratio $q = M_{\mathrm{WR}}/M_{\mathrm{O}}$ is larger than 1. We obtain $q = 2.69 \pm 0.14$ in good agreement with Rauw et al. (1996) who derived $q = 2.78$. Usually, WR stars in binaries are less massive than their companions. Typically, the mass ratio of WR binaries has values between 0.3 and 0.5 (Massey 1981). Only one other system with q larger than unity is known: CQ Cep ($q \sim 1.19$), classified as WN 7 + O by Massey (1981).

Table 4. Physical parameters of WR 22

P [days]	80.336	± 0.0013
e	0.598	± 0.010
γ [$\mathrm{km\,s^{-1}}$]	0	± 15
T_0 [JD 2 400 000.5+]	50 126.97	± 0.14
ω_{WR} [deg]	268.2	± 1.6
$\omega_{\mathrm{O}} = \omega_{\mathrm{WR}} - 180°$ [deg]	88.2	
K_{WR} [$\mathrm{km\,s^{-1}}$]	70.6	± 0.8
K_{O} [$\mathrm{km\,s^{-1}}$]	190	± 10
mass ratio $q = M_{\mathrm{WR}}/M_{\mathrm{O}}$	2.69	± 0.14
$a_{\mathrm{WR}} \sin i$ [10^6 km]	62.5	± 0.9
$a_{\mathrm{O}} \sin i$ [10^6 km]	168.2	± 9.0
$(M_{\mathrm{WR}} + M_{\mathrm{O}}) \sin^3 i$ [$\mathrm{M_\odot}$]	75.9	± 9.0
$M_{\mathrm{O}} \sin^3 i$ [$\mathrm{M_\odot}$]	20.6	± 1.7
$M_{\mathrm{WR}} \sin^3 i$ [$\mathrm{M_\odot}$]	55.3	± 7.3

Usually, WR stars are thought to be in a late stage of stellar evolution and WN stars are expected to be in the helium burning phase (Lamers et al. 1991). However, it has been proposed that the WN 7 stars are still hydrogen burning objects because of their high hydrogen content in their atmospheres (e.g. Crowther et al. 1995). If correct, this implies that there must be a way for a star to become a WR star other than by peeling its outer envelope by mass loss. This alternative way is proposed to be mixing by rotation (Maeder & Zahn 1998; Maeder 1999). The mass-to-luminosity ratio of WR 22 adds evidence to this hypothesis. Crowther et al. (1995) spectroscopically derived a luminosity

Table 5. Comparison of the orbital elements given in the literature with the present results.

Parameter	MS78	N79	CNW79[d]	RVGHMR96	SSSSW98	
P [days]	80.35	80.34	80.35	80.325	80.336	± 0.0013
γ [km s^{-1}]	-23[a]	-28.0	-28	-29.8	0	± 15
e	0.55	0.61	0.64	0.559	0.598	± 0.010
ω [deg]	265	276	275	271.6	268.2	± 1.6
T_0 JD 2 400 000.5+	40 726.7[b]	40 728.4	40 727.8	49 323.67	50 126.97	± 0.14
$K_{\rm WR}$ [km s^{-1}]	70	74	77	72.3	70.6	± 0.8
$K_{\rm O}$[km s^{-1}]	...	...[c]	~ 170[e]	201.4	190	± 10

[a] γ-velocity of N IV λ4058
[b] MS78 give time for passage of WR component in front
[c] N78 found some anti-phase moving absorptions; mass estimation: $M_{\rm WR} \sin^3 i = 64$ M$_\odot$; $M_{\rm O} \sin^3 i = 24$ M$_\odot$
[d] given the solution of Group 1 (Table 7), contains small emission lines of nitrogen and silicon
[e] based on some absorption dips from several Balmer or He II lines
MS78: Moffat & Seggewiss (1978); N79: Niemela (1979); CNW79: Conti et al. (1979);
RVGHMR96: Rauw et al. (1996); SSSSW97: this paper

of $\log(L_{\rm spec}/L_\odot) = 5.8$ (model with $\beta = 1$). Using the stellar evolution tracks of Schaller et al. (1992) we find that the parameters of WR 22 fit to a model characterized by $M_{\rm ini} = 60\,{\rm M}_\odot$ and $Z = 0.020$. At time-step 7, at an age of about 2.5 Myr, the theory of stellar evolution predicts a mass of $55.6\,{\rm M}_\odot$ and a luminosity of $\log L/L_\odot = 5.9$. In this model, the star is still in the core H-burning phase ($X_c \simeq 0.22$). We note that there is also a remarkably good agreement of the theoretically calculated radius and effective temperature with the observed values: $R_{2/3} = 28.5$ R$_\odot$, $T_{\rm eff} = 31.2$ kK (Crowther et al. 1995). Of course, stellar evolution without accounting for mixing by rotation does not predict that a star in such an early phase of its evolution looks like a Wolf-Rayet star. On the other hand, if WR 22 were a classical Wolf-Rayet star in a He-burning phase, then its mass would imply a luminosity of $\log L_{\rm evol}/L_\odot = 6.5$ (Schaerer & Maeder 1992), which is a factor of 5 larger than what is inferred from the observations.

For most of the orbital parameters of WR 22 the present results are consistent with earlier investigations. However, the good quality of our observational data and the excellent coverage of the orbital period allows to tighten the errors of the measurements. The controversial parameters for which we disagree with previous determinations are the velocity amplitude of the O companion and the eccentricity of the orbit (see Table 5). We derive $e = 0.598 \pm 0.010$. The difference to the value obtained by Rauw et al. (1996), $e = 0.559 \pm 0.009$, is significant and has consequences for the mass determination.

The orbital movement of the companion is difficult to detect. With different methods, we derive $K_{\rm O} \sim 190$ km s^{-1} which is less than the determination of Rauw et al. (1996) and significantly larger than the estimate of Conti et al. (1979) (see Table 5). Because of the revised values for the eccentricity and the semi-amplitude we revise down the previously determined mass of the WR star by Rauw et al. (1996), $M_{\rm WR} = 72\,{\rm M}_\odot$, to the substantially smaller mass of $M_{\rm WR} = 55\,{\rm M}_\odot$.

We were fortunate to obtain observations that cover more than one orbit with high time resolution. This is not trivial for a binary such as WR 22 with a period of 80 days. Our data allowed us to improve the orbital parameters. However, despite our correction to the mass of the Wolf-Rayet star we still concur with Rauw et al. (1996) that WR 22 is "the most massive Wolf-Rayet star ever weighed." This property makes WR 22 an outstanding object that in our opinion justifies the extraordinary efforts that were needed to collect the observations presented in this paper.

Acknowledgements. We thank the staff at La Silla for their assistance and we acknowledge the contributions of Drs. T. Dumm, A. Kaufer, H. Lehmann, J. Peitz, and Th. Rivinius, who were observers during the observing campaign. The construction of the spectrograph HEROS was supported by the Deutsche Forschungsgemeinschaft (Wo 296/20-1) and J.S. acknowledges the grant Wo 296/22-1,3.

References

Balona L.A., Egan J., Marang F., 1989, MNRAS 240, 103
Conti P.S., Alschuler W.R., 1971, ApJ 170, 325
Conti P.S., Niemela V.S., Walborn N.R., 1979, ApJ 228, 206
Crowther P.A., Smith L.J., Hillier D.J., Schmutz W., 1995, A&A 293, 427
Gosset E., Remy M., Manfroid J., et al., 1991, Inf. Bull. Var. Stars 3571
Hamann W.-R., Dünnebeil G., Koesterke L., Schmutz W., Wessolowski U., 1991, A&A 249, 443
Howarth I.D., Prinja R.K., 1989, ApJS 69, 527
Kaufer A., Stahl O., Wolf B., et al., 1996, A&A 305, 887
Kaufer A., Stahl O., Wolf B., et al., 1997, A&A 320, 273
Kaufer A., 1998, Variable circumstellar structure of luminous hot stars: the impact of spectroscopic long-term campaigns. In: Schielicke R.E. (ed.) Reviews of Modern Astronomy Vol. 11, Astronomische Gesellschaft, p. 177
Lamers H.J.G.L.M., Maeder A., Schmutz W., Cassinelli J.P., 1991, ApJ 368, 538
Lundström I., Stenholm B., 1984, A&AS 58, 163
Maeder A., 1999. In: van der Hucht K.A., Koenigsberger G., Eenens P.R.J. (eds.) Proc. IAU Symp. 193, Wolf-Rayet phenomena in massive stars and starburst galaxies. ASP, San Francisco, p. 177
Maeder A., Zahn J.-P., 1998, A&A 334, 1000
Massey P., 1981, ApJ 246, 153
Mathys G., 1988, A&AS 76, 427

Moffat A.F.J., Seggewiss W., 1978, A&A 70, 69
Niemela V.S., 1973, PASP 85, 220
Niemela V.S., 1979. In: Conti P.S., de Loore C.W.H. (eds.) Proc. IAU Symp. 83, Mass Loss and Evolution of O-Type Stars. Reidel, Dordrecht, p. 291
Press W.H., Teukolsky S.A., Vetterling W.T., Flannery B.P., 1992, Numerical Recipes in C. Cambridge University Press, Cambridge
Rauw G., Vreux J.-M., Gosset E., et al., 1996, A&A 306, 771
Schaerer D., Maeder A., 1992, A&A 263, 129
Schaller G., Schaerer D., Meynet G., Maeder A., 1992, A&AS 96, 269
Schmutz W., Vacca W.D., 1991, A&A 248, 678
Smith L.F., 1968, MNRAS 140, 409
Stahl O., Kaufer A., Wolf B., et al., 1995, The Journal of Astronomical Data 1, 3 (on CD-ROM)
van der Hucht K.A., Conti P.S., Lundström I., Stenholm B., 1981, Space Sci. Rev. 28, 227
van der Hucht K.A., Hidayat B., Admiranto A.G., Supelli K.R., Doom C., 1988, A&A 199, 217